

Early and Prediagnostic Detection of Pancreatic Cancer from Computed Tomography

Wenxuan Li^{1†}, Pedro R. A. S. Bassi^{1,2,3†}, Lizhou Wu^{4†},
Xinze Zhou^{1†}, Yuxuan Zhao^{5†}, Qi Chen^{1†}, Szymon Płotka^{6†},
Tianyu Lin¹, Zheren Zhu^{7,8}, Marisa Martin⁷, Justin Caskey⁷,
Shanshan Jiang⁹, Xiaoxi Chen¹⁰, Jarosław B. Ćwikła¹¹,
Artur Sankowski¹², Yaping Wu¹³, Tom Lu¹⁴, Ebenezer Daniel¹⁴,
Sergio Decherchi³, Andrea Cavalli^{2,3,15}, Chandana Lall¹⁴,
Cristian Tomasetti¹⁴, Yaxing Guo¹³, Xuan Yu¹³, Yuqing Cai¹⁶,
Hualin Qiao¹⁷, Jie Bao¹⁸, Chenhan Hu¹⁸, Ximing Wang¹⁸,
Arkadiusz Sitek^{19,20}, Kai Ding⁹, Heng Li⁹, Meiyun Wang^{13,21*},
Dexin Yu^{5*}, Guang Zhang^{4*}, Yang Yang^{7*}, Kang Wang^{7*},
Alan L. Yuille^{1*}, Zongwei Zhou^{1*}

¹Johns Hopkins University, Baltimore, MD, USA.

²University of Bologna, Bologna, Italy.

³Istituto Italiano di Tecnologia, Genova, Italy.

⁴Shandong Provincial Qianfoshan Hospital, Shandong, China.

⁵Qilu Hospital of Shandong University, Shandong, China.

⁶Jagiellonian University, Krakow, Poland.

⁷University of California, San Francisco, CA, USA.

⁸University of California, Berkeley, CA, USA.

⁹Johns Hopkins Medicine, Baltimore, MD, USA.

¹⁰University of Illinois Urbana-Champaign, IL, USA.

¹¹University of Warmia and Mazury, Olsztyn, Poland.

¹²National Medical Institute of the Ministry of Internal Affairs and Administration, Warsaw, Poland.

¹³Henan Provincial People's Hospital & The People's Hospital of Zhengzhou University, Zhengzhou, China.

¹⁴City of Hope National Medical Center, Duarte, CA, USA.

¹⁵Centre Européen de Calcul Atomique et Moléculaire, École Polytechnique Fédérale de Lausanne, Lausanne, Switzerland.

¹⁶Northeastern University, Boston, MA, USA.

¹⁷Rutgers University, New Brunswick, NJ, USA.

¹⁸The First Affiliated Hospital of Soochow University, Soochow, China.

¹⁹Massachusetts General Hospital, Boston, MA, USA.

²⁰Harvard University, Cambridge, MA, USA.

²¹Biomedical Research Institute, Henan Academy of Sciences,
Zhengzhou, China.

*Corresponding author(s). E-mail(s): zzhou82@jh.edu;

†These authors contributed equally to this work.

Abstract

Pancreatic ductal adenocarcinoma (PDAC), one of the deadliest solid malignancies, is often detected at a late and inoperable stage. Retrospective reviews of prediagnostic CT scans, when conducted by expert radiologists aware that the patient later developed PDAC, frequently reveal lesions that were previously overlooked. To help detecting these lesions earlier, we developed an automated system named ePAI (early Pancreatic cancer detection with Artificial Intelligence). It was trained on data from 1,598 patients from a single medical center. In the internal test involving 1,009 patients, ePAI achieved an area under the receiver operating characteristic curve (AUC) of 0.939–0.999, a sensitivity of 95.3%, and a specificity of 98.7% for detecting small PDAC less than 2 cm in diameter, precisely localizing PDAC as small as 2 mm. In an external test involving 7,158 patients across 6 centers, ePAI achieved an AUC of 0.918–0.945, a sensitivity of 91.5%, and a specificity of 88.0%, precisely localizing PDAC as small as 5 mm. Importantly, ePAI detected PDACs on prediagnostic CT scans obtained 3 to 36 months before clinical diagnosis that had originally been overlooked by radiologists. It successfully detected and localized PDACs in 75 of 159 patients, with a median lead time of 347 days before clinical diagnosis. Our multi-reader study showed that ePAI significantly outperformed 30 radiologists by 50.3% ($P < 0.05$) in sensitivity while maintaining a comparable specificity of 95.4% in detecting PDACs early and prediagnostic. These findings suggest its potential of ePAI as an assistive tool to improve early detection of pancreatic cancer.

1 Main

Pancreatic ductal adenocarcinoma (PDAC) is one of the deadliest cancers worldwide. Each year, more than 495,000 new cases diagnosed globally, and almost the same number of patients die from the disease, highlighting its exceptionally high fatality rate. Despite advances in cancer treatment, the overall five-year survival rate of PDAC remains around 13% [1].

Survival is low largely because early detection is uncommon. In most patients, PDAC is detected only after it has already spread beyond the pancreas, when curative treatment is no longer possible. In contrast, when PDAC is detected while still localized to the pancreas, five-year survival increases to approximately 40–45%, compared with about 3% when detection occurs after distant spread.

Computed tomography (CT) offers a scalable path because it is already used at massive global volume: about 300 million CT examinations are performed worldwide each year, and roughly 40% are contrast-enhanced. Even if only a subset are contrast-enhanced abdominal CT, this still corresponds to tens of millions of scans per year worldwide that already include the pancreas. This scale creates a practical opportunity for opportunistic detection of PDAC on scans obtained for other clinical reasons, while also providing spatial localization that blood-based tests and molecular assays cannot.

However, CT alone has not proven effective for detecting small, early-stage cancers or precancerous lesions. Recognizing subtle early changes is difficult, even for experienced radiologists. Because most abdominal CT scans are performed for non-pancreatic indications, radiologists may not sufficiently focus on the pancreas. When radiologists retrospectively review prediagnostic CT scans, their sensitivity is often low, and agreement between readers is limited. For example, Mukherjee et al. [2] reported sensitivities of only 33.3% and 31.1% among two radiologists. These results highlight the limits of visual interpretation using conventional methods.

Several retrospective studies have shown that early signs of PDAC are often present on CT scans months or even years before clinical diagnosis. These signs include pancreatic duct dilatation, pancreatic atrophy, and focal intrapancreatic late enhancement. Across studies, such findings were visible in 16% to 71% of prediagnostic CT scans obtained 3 to 36 months before diagnosis [3–7]. These observations suggest that prediagnostic CT scans contain valuable information for detecting PDAC at an earlier and potentially more treatable stage.

This gap between the diagnostic potential of prediagnostic CT scans and human performance points to a clear need for computational assistance. Artificial intelligence (AI) is well suited for this role. AI has achieved expert-level performance in many cancer detection tasks [8–11]. However, relatively few studies have focused on early or small PDAC detection on CT scans. Existing studies are often evaluated on very small cohorts, and performance on small tumors is limited [12–17]. The reported sensitivities range from 74.7% to 85.7%, but these results are based on only tens of patients. Importantly, these studies are evaluated on diagnostic CT scans, not on prediagnostic scans acquired before clinical detection.

Existing studies have limitations. **First**, many studies are trained and tested using data from a single population or geographic region [12, 14, 15, 17]. This limits generalizability, as models trained on one population may not perform reliably on patients from different ethnic or clinical backgrounds. **Second**, reproducibility remains a major challenge. Many studies rely on private datasets for both training and testing, and the trained models are not publicly released [12–15, 18]. As a result, independent validation is difficult, fair comparison across methods is not possible, and reported performance cannot be easily reproduced. **Third**, many existing approaches focus on

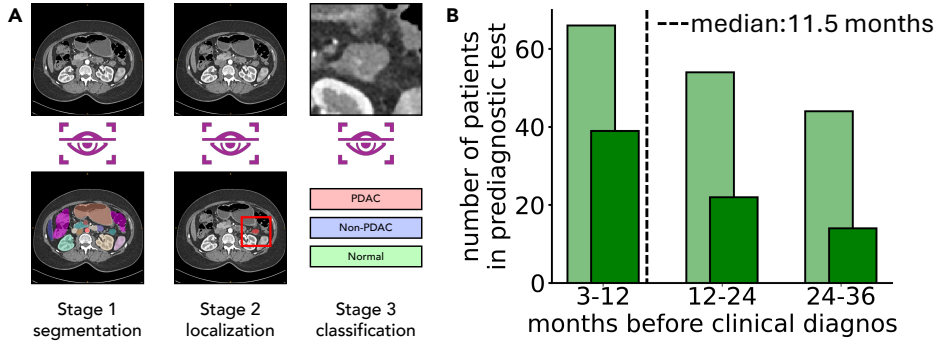


Fig. 1: Overview and performance of the ePAI system. A. The ePAI system detects pancreatic ductal adenocarcinoma (PDAC) through a three-stage cascade: Stage 1 segments pancreatic and surrounding anatomy, Stage 2 localizes all potential lesions, and Stage 3 classifies each lesion as PDAC, non-PDAC, or normal. **B.** Distribution of number of detections in prediagnostic CT scans, showing that ePAI identified PDAC a median of 347 days before the first clinical diagnosis by radiologists.

patient-level prediction without lesion localization [13, 14, 17, 18]. Without localization, it is unclear whether a model bases its decision on pancreatic findings or on unrelated image features. Clinically, the lack of localization also prevents users from knowing where a suspicious lesion is located, which limits interpretability and practical usefulness.

To address this, we have developed an open-source, automated system, ePAI (early Pancreatic cancer detection with Artificial Intelligence), which detects and localizes small PDACs less than 2 cm in diameter with high accuracy not only in diagnostic scans but also in prediagnostic scans taken 3 to 36 months before clinical diagnosis. This will result in safe and effective detection of early-stage malignancies missed by standard of care diagnostic techniques, and in some cases will enable timely treatment with intent to cure. Our study first evaluated ePAI internally on abdominal contrast-enhanced CT scans, consisting of 1,009 patients, and then validated ePAI on a larger external multicenter test cohort, consisting of 7,158 patients, to assess its generalizability to various settings. Furthermore, we study the feasibility of applying ePAI on prediagnostic CT scans, collected 3–36 months before clinical diagnosis, and compare its performance with results from a multi-reader study involving 30 radiologists in early and prediagnostic detection of pancreatic cancer.

2 Results

2.1 The ePAI system

We present ePAI, an automated system for detecting and localizing PDAC from contrast-enhanced CT scans. ePAI performs three main tasks: detecting the presence of pancreatic lesions, segmenting the lesion, and classifying lesions as PDAC or non-PDAC (Figure 1A).

ePAI was trained on a dataset of contrast-enhanced abdominal CT scans from 1,598 patients at Johns Hopkins Hospital (JHH) [19, 20]. Patient characteristics are summarized in Table A2. Ground truth labels were confirmed by surgical pathology for lesion cases and by two-year follow-up for normal controls. ePAI was supervised with pixel-wise annotations of the pancreas and lesions provided by radiologists. To enhance sensitivity, especially for detecting and localizing very small lesions, ePAI was additionally trained on a large set of synthetic lesions with pixel-wise annotations automatically provided by generative AI [21–24]. Further details on the dataset and annotations are provided in the Methods section.

The ePAI system is structured as a three-stage cascade designed to enhance model interpretability, adaptability to varying lesion types and anatomical structures, and performance across tasks of increasing complexity. Stage 1: An nnU-Net model [25] was used for anatomical segmentation to localize the pancreas (head, body, tail), surrounding vessels (arteries and veins), and visible dilated ducts. Stage 2: The same nnU-Net model was fine-tuned to detect and localize all potential pancreatic lesions on contrast-enhanced CT scans. It was trained on both real and synthetic lesions to improve sensitivity and included a large cohort of normal scans to reduce false positives and enhance specificity. Stage 3: A classification model analyzed the detected lesions using features like their shape, texture, location, and pancreas morphology (including radiomics features and AI features), allowing for classification among PDAC, non-PDAC lesions and normal.

We mainly evaluated ePAI in detecting and localizing PDACs, with a special focus on small PDACs (≤ 2 cm). The evaluation was conducted on two types of contrast-enhanced CT scans: (1) **diagnostic scans** where radiologists correctly detected and reported PDACs, and (2) **prediagnostic scans** where radiologists initially overlooked the PDACs, which were only detected and reported in follow-up scans 3–36 months later. ePAI was an interpretable AI model that directly outputs the segmentation mask of the pancreas, surrounding vessels, dilated ducts and pancreatic lesions if present. Two tasks were evaluated. The first task is PDAC detection: that is, PDAC versus normal, which also includes detection rates stratified by cancer stage. The second task is PDAC localization: a lesion was considered correctly localized only if its position matched the radiologists' voxel-wise annotations or descriptions in the reports.

2.2 Early detection and localization of PDACs from internal test cohort

Our internal test cohort consisted of 1,009 patients (279 patients with PDAC, 427 patients with non-PDAC, and 303 normal controls) from JHH. These patient labels were confirmed on surgical pathology or a 2-year follow-up.

We first evaluated PDAC detection at the *patient* level. For all-size PDAC detection, ePAI achieved an area under the receiver operating characteristic curve (AUC) of 0.985 (95% confidence interval (CI): 0.974–0.994), a sensitivity of 97.1% (95% CI: 94.4–98.5%), and a specificity of 98.7% (95% CI: 96.6–99.5%) as shown in Figure 2A–B. The sensitivity for detecting small PDACs (diameter ≤ 2 cm) was 95.3% (95% CI: 84.5–98.7%; n = 43), precisely detecting PDAC as small as 2 mm; for detecting large PDACs (diameter > 2 cm) was 97.5% (95% CI: 94.6–98.8%; n = 236). ePAI achieved

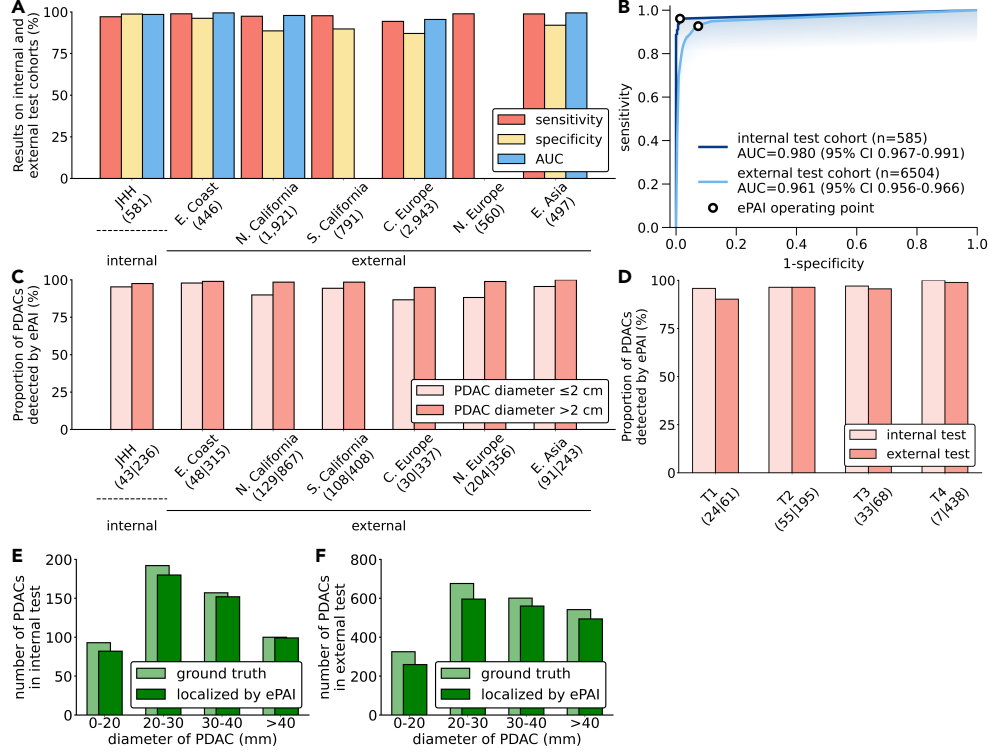


Fig. 2: Internal and external validation of early PDAC detection with ePAI.

(A) Sensitivity, specificity, and area under the receiver operating characteristic curve (AUC) of ePAI for detecting all-size PDAC in the internal test cohort and six external regional multicenter test cohorts. (B) Receiver operating characteristic (ROC) curves of ePAI for detecting all-size PDAC across internal and external cohorts, highlighting its generalizability across centers. (C) Sensitivity of ePAI stratified by PDAC lesion size (≤ 2 cm vs. > 2 cm). (D) Sensitivity stratified by PDAC T-stage (T1–T4), showing strong performance even in the earliest stages. Localization performance in internal (E) and external cohorts (F), evaluated by localization accuracy between the predicted lesion location and radiologists' voxel-wise annotations or report-based localization, ePAI achieved 94.6% in internal test cohort while achieved 88.7% in external test cohort.

a sensitivity of 95.8% (95% CI: 79.8–99.3%; $n = 24$) for T1 stage, 96.4% (95% CI: 87.7–99.0%; $n = 55$) for T2 stage, and 97.5% (95% CI: 87.1–99.6%; $n = 40$) for T3–4 stage (Figure 2C).

We further evaluated PDAC localization at the *lesion* level. Localization was measured whether the model correctly identifies the spatial location of a PDAC lesion. A predicted PDAC was considered correctly localized if it overlapped with the radiologists' voxel-wise annotated tumor mask. We obtained a sensitivity of 94.6% (95%

CI: 92.4–96.1%; n = 542) for localization of all-size PDACs and 88.2% (95% CI: 80.0–93.3%; n = 93) for small PDACs (Figure 2E).

2.3 Early detection and localization of PDACs from external multicenter test cohorts

To assess the generalizability of ePAI to different patient populations and imaging protocols, we validated our model on external multicenter (n = 6) test cohorts, which consisted of contrast-enhanced abdominal CT scans of 7,158 patients (610 with small PDAC, 2,529 with large PDAC, and 4,019 normal controls) from North America, Europe, and Asia. The patient labels were confirmed by histopathology reports or a 2-year follow-up visit diagnosis.

ePAI achieved an AUC of 0.971 (95% CI: 0.967–0.976), sensitivity of 97.0% (95% CI: 96.1–97.6%), and specificity of 88.0% (95% CI: 87.0–89.0%) for all size PDAC detection. For the small PDAC patient subgroup (diameter \leq 2 cm), the sensitivity was 91.5% (95% CI: 89.0–93.4%; n = 610). For the large PDAC patient sub-group (diameter $>$ 2 cm), the sensitivity was 98.3% (95% CI: 97.7–98.7%; n = 2,529). The PDAC detection results for each center are shown in Figure 2A–C. ePAI achieved a sensitivity of 90.2% (95% CI: 80.2–95.4%; n = 61) for T1, 96.4% (95% CI: 92.8–98.3%; n = 195) for T2, and 98.4% (95% CI: 96.9–99.2%; n = 506) for T3–4. We obtained a sensitivity of 88.7% (95% CI: 87.4–89.9%; n = 2,404) for localization of all-size PDACs and 79.7% (95% CI: 75.3–84.1%; n = 325) for small PDACs (Figure 2F).

2.4 Prediagnostic detection and localization of PDACs from external multicenter test cohorts

To investigate whether ePAI can detect PDAC before radiologists, we tested it on CT scans acquired 3–36 months prior to the first clinical diagnosis by radiologists. These scans are called prediagnostic scans. External multicenter (n = 3) test cohorts were collected from North America and Eastern Asia, including 159 patients with both prediagnostic and diagnostic CT scans. This cohort was eventually diagnosed with PDAC. Unfortunately, in practice, radiologists failed to detect PDACs in 100% of these prediagnostic scans, indicating that these lesions were retrospectively visible but initially overlooked. The diagnostic scans from this same cohort showed advanced disease, with an average stage of 2.67 and a mean tumor diameter of 3.1 ± 1.5 cm. The normal controls remained the same as those used for external validation of early PDAC detection (Section 2.3).

Without additional training or parameter adjustment on prediagnostic CT scans, ePAI successfully detected PDAC in 75 out of 159 patients, with a median leading time of 347 days before first clinical diagnosis by radiologists. Localization accuracy was assessed by comparing predicted PDAC sites in prediagnostic scans with the confirmed PDAC locations in diagnostic scans (Figure 3A). Localization was considered correct when the predicted region corresponded to the same pancreatic segment (head, body, or tail) as in the diagnostic scan. ePAI correctly localized PDAC in 75% of the patients whose tumors were directly detected. Moreover, ePAI identified secondary morphological changes like pancreatic-duct dilation in 85% of the patients

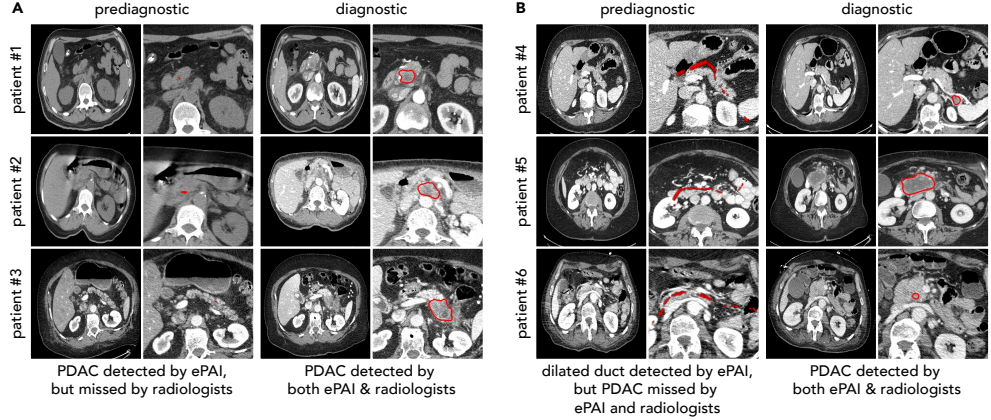


Fig. 3: Earlier PDAC detection in prediagnostic CT scans. Representative paired prediagnostic (left) and diagnostic (right) contrast-enhanced CT images from six patients in the external multicenter prediagnostic cohorts (3–36 months before first clinical diagnosis). Red contours indicate ePAI predictions or radiologist-confirmed tumor regions on the diagnostic scans. **(A)** Patients #1–#3 show *direct prediagnostic detection*: ePAI marks small, subtle abnormalities on the prediagnostic scans (small red contours), and the diagnostic scans later show an obvious PDAC at the same location (red contours), detected by both ePAI and radiologists. **(B)** Patients #4–#6 show *indirect prediagnostic cues*: ePAI highlights secondary changes on the prediagnostic scans, most notably pancreatic duct dilatation or cutoff (red 3D rendering), even when no clear mass is visible to ePAI or radiologists. The paired diagnostic scans later show a clear PDAC (red contour) detected by both ePAI and radiologists. Together, these examples illustrate two common prediagnostic patterns—early subtle lesions and secondary ductal changes before an obvious mass—and potentially support the use of ePAI for earlier PDAC review.

whose tumors were not directly detected (Figure 3B). These findings indicate that ePAI can recognize early structural alterations preceding overt tumor visibility.

2.5 Multi-reader study and comparison between ePAI and radiologists

We conducted a multi-reader study to compare performance of ePAI with radiologists in detecting early PDAC less than 2 cm. A total of 30 readers (median years of experience: 4, mean: 6.1, s.d.: 7.5, range: 2–37) participated in the study. The readers included pancreas specialists ($n = 3$), general radiologists ($n = 12$), and radiology residents ($n = 15$) recruited from Johns Hopkins Medicine (JHMI), City of Hope (CoH), the University of California, San Francisco (UCSF), the University of Illinois Urbana–Champaign (UIUC), Shandong Provincial Qianfoshan Hospital (SFMU), and Qilu Hospital of Shandong University (QLH).

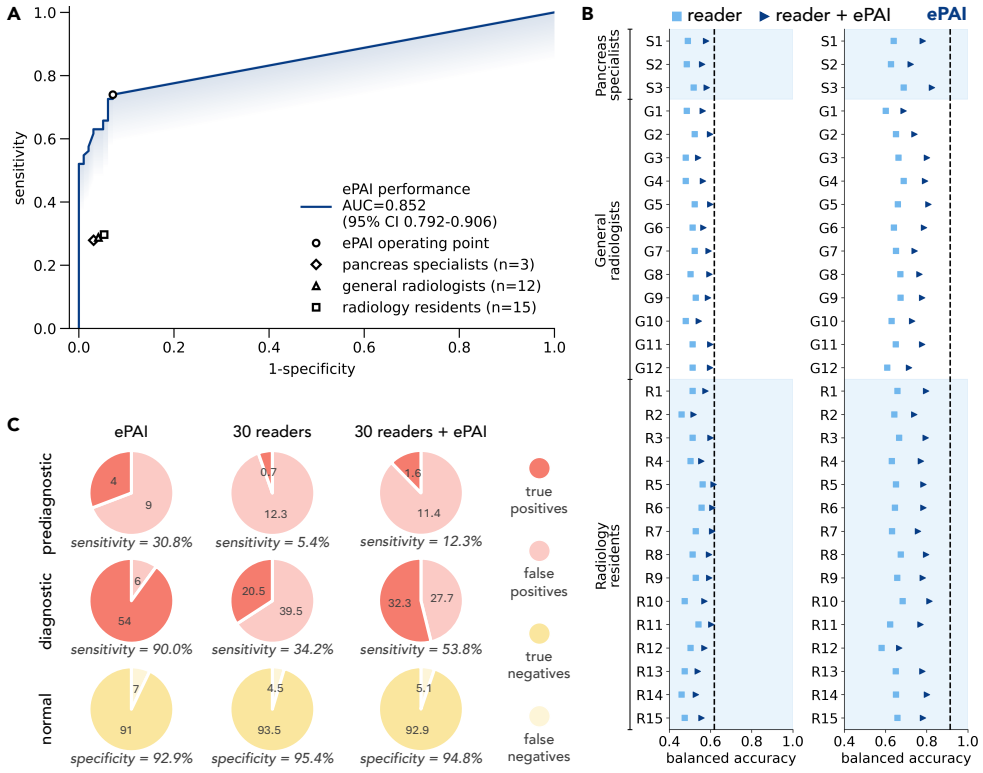


Fig. 4: Multi-reader study. (A) Comparison between ePAI and 30 readers with different expertise, evaluated on prediagnostic, diagnostic, and normal CT scans. ePAI shows substantially higher sensitivity in both prediagnostic and diagnostic settings while maintaining high specificity on normal controls. (B) Balanced accuracy of individual readers (pancreatic imaging specialists, general radiologists, and radiology residents) compared with ePAI and themselves with assistance of ePAI. (C) Sensitivity, specificity of ePAI, readers, and reader-plus-ePAI combinations for prediagnostic, diagnostic, and normal cohorts.

Both ePAI and human readers reviewed a mixed cohort including 13 prediagnostic and 63 diagnostic CT scans with early PDACs, as well as 99 normal CT scans with at least 2 years follow-up as controls. This proportion is unknown to the readers beforehand. Readers reviewed all the CT scans and rated each case as PDAC or normal. The results in Figure 4 showed that ePAI outperformed 30 radiologists by 50.3% (95% CI: 37.6–62.1%) in sensitivity while maintaining more than 92.0% specificity in detecting PDACs early and prediagnostic. Specifically, for diagnostic scans, ePAI achieved a sensitivity of 90.0%, markedly higher than the average of 34.2% among the 30 readers. For prediagnostic scans, ePAI detected 30.8% of PDACs that were initially missed by radiologists, compared with only 5.4% detected by readers after they re-reviewed these scans. When assisted by ePAI, radiologists improved sensitivity by

19.6% and 6.9% in diagnostic and prediagnostic scans, respectively. Collectively, these results demonstrate that ePAI substantially outperforms human readers in early and prediagnostic PDAC detection while achieving a similar specificity on normal cases.

3 Discussion

We observed strong performance of ePAI for PDAC detection and localization, with robust generalization across external cohorts and substantial improvement over radiologists. With 94.4%–98.5% sensitivity and 96.6%–99.5% specificity, ePAI reached clinically meaningful positive predictive value (PPV) in enriched high-risk populations with PDAC prevalence of 3.6%–4.4% [26–28], yielding a PPV of 50.9%–90.0%. In this setting, screening 100,000 individuals would identify approximately 3,398–4,334 true positives among 4,812–6,676 AI-flagged cases. In contrast, PDAC is rare in the general population. At low-risk prevalence levels (0.014%–0.03%) [29–31], screening 100,000 individuals would yield only 13–30 true positives among 530–3,413 positive predictions (PPV: 0.4%–5.6%), meaning that the vast majority of flagged cases would be false positives.

Recent AI studies on pancreatic cancer detection have only been tested on single population or very limited geographic regions [12–17], restricting evaluation of generalizability. In contrast, we conducted large-scale external validation across six independent regional cohorts spanning North America, Europe, and Asia, including a national registry from Poland aggregating data from more than 60 hospitals. This design enables robust assessment across heterogeneous patient populations, scanner vendors, and acquisition protocols. Detection of small tumors ≤ 2 cm is clinically important because these tumors are more likely to be surgically resectable. Unlike most prior work, which either did not report performance on small tumors [17] or included only a few such cases [12], we conducted extensive subgroup analyses on 653 patients with small tumors, demonstrating that ePAI maintains high sensitivity for early-stage PDACs. The observed robustness is supported by the training design and supervision signals used in this study, including synthetic tumor augmentation and rich voxel-wise annotations that provide anatomical context beyond the tumor itself (e.g., pancreas and pancreatic sub-regions, pancreatic duct, adjacent vessels, and surrounding organs).

Compared with PDAC detection, tumor localization has received far less systematic evaluation in the literature. Most prior studies focus on patient-level classification and, at most, provide qualitative visualization tools such as saliency maps or heatmaps, often assessed on a limited number of cases without explicit anatomical ground truth. In this study, we define localization as correctly identifying the pancreatic region (head, body, or tail) containing the tumor, and we evaluate this capability using voxel-wise tumor annotations in the internal cohort and anatomically defined pancreatic segments in external cohorts. ePAI correctly localizes more than 90% of detected tumors to the appropriate pancreatic region. This represents one of the most comprehensive quantitative evaluations of PDAC localization to date. Localization is clinically important because it reduces radiologist search burden, mitigates perceptual errors, and enables actionable downstream decisions, such

as targeted endoscopic ultrasound-guided biopsy. More broadly, localization distinguishes imaging-based approaches from non-imaging early-detection methods, such as blood-based or molecular assays, which may indicate elevated cancer risk but cannot specify the organ or anatomical site of disease. By providing spatially resolved information, ePAI bridges the gap between early cancer suspicion and organ-specific clinical workup.

A central contribution of this study is the evaluation of ePAI on prediagnostic CT scans acquired between 3 and 36 months before clinical diagnosis. This is one of the most clinically important—and technically difficult—settings for early PDAC detection: abnormalities are often subtle, indirect, or not yet a discrete mass. In our external prediagnostic cohort (159 patients with paired prediagnostic and diagnostic scans), radiologists did not report PDAC in any prediagnostic scan at the time of care, whereas ePAI detected PDAC in 75/159 patients with a median lead time of 347 days and localized the predicted site to the correct pancreatic segment (head/body/tail) in 75% of detected cases. These findings highlight two distinct clinical scenarios that explain why PDAC is missed in practice. First, the radiologist may be “correct” under a lesion-centric standard: the scan may not contain a clearly actionable tumor, but may show early or non-specific precancerous or high-risk morphologic changes (e.g., subtle focal abnormalities) that would justify risk stratification and closer surveillance rather than immediate biopsy or intervention. Second, the radiologist may be “incorrect” in the sense of perceptual or cognitive miss: an already visible abnormality is overlooked or dismissed, leading to delayed workup and subsequent imaging or surgery once the disease becomes obvious. Additional contributors include time pressure in routine abdominal CT interpretation, attention competition from non-pancreatic findings, protocol and image-quality variability (contrast timing, slice thickness, partial pancreatic coverage), lack of explicit prompts to scrutinize the pancreas when the indication is unrelated, and the fact that early PDAC may present primarily through secondary signs rather than a conspicuous mass. By flagging suspicious regions and related structural cues (including pancreatic-duct changes), ePAI can shift care from passive detection to proactive risk-aware follow-up—either prompting earlier targeted review when a lesion is already present, or supporting earlier surveillance when only subtle high-risk changes exist.

The multi-reader study underscores the persistent difficulty of detecting early PDAC. Radiologists across training levels showed low sensitivity for small and prediagnostic tumors, consistent with performance reported in the literature. AI assistance improved sensitivity for all readers, including those without subspecialty experience, and maintained high specificity on normal scans. These findings align with established benefits of AI-augmented interpretation in other screening domains, such as lung nodules and breast cancer. They support the emerging concept that opportunistic AI review of abdominal CT scans may enable earlier PDAC detection by drawing attention to subtle abnormalities that would otherwise be missed.

These results carry several implications for opportunistic PDAC detection. First, the consistent performance of ePAI across multiple regional centers—including, but not limited to, Northern California—suggests feasibility for broad deployment. Second, strong localization performance may help radiologists confirm or refute abnormalities

quickly without extended search. Third, the ability to detect PDAC prior to clinical diagnosis indicates potential for earlier identification, though further refinement and prospective validation are required. Given the low prevalence of PDAC, integrating ePAI with clinical risk models (e.g., ENDPAC) or laboratory markers to identify higher-risk populations may reduce false positives while maximizing benefit. Evaluating downstream consequences of AI-generated alerts, including follow-up imaging and invasive procedures, will be essential.

In one of our six multicenter external test cohorts, Northern California dataset, we made it scale by using large language models (LLMs) to assist in identifying normal controls, path-proven PDAC cases, and prediagnostic scans, followed by expert verification. This workflow highlights the value of LLMs for accelerating data curation, a major bottleneck in developing medical imaging AI systems, and aligns with emerging evidence that agentic LLM pipelines can support large-scale clinical dataset assembly.

Our study has limitations. Clinical information was incomplete for some external sites, limiting certain subgroup analyses. The multi-reader study did not measure interpretation time, preventing direct assessment of workflow efficiency. Finally, performance varied across centers, likely reflecting heterogeneity in scanners, protocols, and contrast timing. Future work should address these domain shifts and evaluate ePAI in prospective clinical settings.

4 Methods

4.1 Dataset description

This multicenter retrospective study comprised five patient cohorts: **(I)** an internal training cohort of diagnostic CT scans for model development; **(II)** an internal test cohort of diagnostic CT scans for performance evaluation; **(III)** an external multicenter diagnostic CT cohort ($n = 6$) for generalization assessment; **(IV)** an external multicenter prediagnostic CT cohort ($n = 3$); and **(V)** an external multicenter reader-study cohort including diagnostic, prediagnostic, and normal scans. Across all cohorts, PDAC was confirmed by pathology, including histopathology of surgical specimens or cytology when surgery was not performed, followed the 2019 WHO Classification of Tumors [32]. Patients with mixed neoplasms (e.g., PDAC with neuroendocrine or cystic components) were excluded. Normal controls were confirmed to be free of pancreatic disease, and patients with acute pancreatitis or prior abdominal treatment were excluded.

Internal training and testing cohorts (Cohorts I & II) comprised 2,519 patients, each patient with dual-phase contrast-enhanced CT scans acquired in the arterial and portal-venous phases, resulting in a total of 5,085 annotated CT scans. All scans were pancreatic-protocol CTs acquired on Siemens multidetector CT scanners. This retrospective study was approved by the Johns Hopkins Hospital Institutional Review Board under IRB00403268. Diagnostic CT scans included 3,440 scans acquired between 2003 and 2020 and identified from clinical, radiology, and pathology databases. Among these, 864 patients had pathology-confirmed PDAC, including 576 patients in Cohort I and 288 patients in Cohort II, with PDAC tumors stratified by size (≤ 2 cm vs. > 2 cm) as summarized in Table A2. The remaining diagnostic

scans corresponded to non-PDAC pancreatic diseases. Normal controls consisted of 1,645 CT scans from 836 renal donor patients without pancreatic tumors, including 533 patients in Cohort I and 303 patients in Cohort II. To minimize the likelihood of undiagnosed pancreatic disease, 99% of renal donor scans were acquired before 2010. Both arterial and portal-venous phases were independently used for model training.

Lesion and pancreas annotation. The entire three-dimensional pancreas and PDAC tumors were manually segmented by five trained annotators using commercial segmentation software 3D Slicer for Cohorts I and II. For subjects with dual-phase CT scans, pancreas and PDAC tumors were independently annotated in both arterial and portal-venous phases by a single annotator with around 2 years in experience post residency. All annotations were subsequently reviewed and verified by one of three board-certified radiologists who were not involved in the initial segmentation. To mitigate the impact of annotation errors and inter- or intra-observer variability on model training and evaluation, a dedicated quality control and error-correction procedure was applied. Potential annotation errors were first identified through expert visual inspection and then systematically screened using in-house software to detect major inconsistencies, such as missing slices or incomplete organ coverage within the region of interest. Radiologist re-review was conducted to correct errors in the ground truth, including missed small PDAC tumors and slight inaccuracies in their locations.

External multicenter test cohorts (Cohorts III). Independent evaluation of model generalization was performed using external multicenter test cohorts (Cohort III) comprising 7,158 patients from the North America, Europe, and Eastern Asia, including 3,139 PDAC cases and 4,019 normal controls (Tables A1-A3). Data sources were grouped by geographic region. All external cohorts were fully held out from model training and validation. The East Coast (North America) cohort included 446 patients, comprising 363 diagnostic PDAC cases and 80 normal controls. Diagnostic cases were confirmed by histopathology. Normal controls were defined by the absence of pancreatic malignancy or major abdominal pathology. Normal scans were acquired exclusively in the portal-venous phase, with a median in-plane spacing of 0.86 mm and a slice thickness of 1.0 mm. The mean age of normal subjects was 46.8 ± 16.7 years, with 33.8% female and 66.2% male participants. The Northern California (North America) comprised 1,921 patients, including 996 diagnostic PDAC cases and 952 normal controls. Diagnostic cases had a mean age of 65.4 ± 10.7 years and included 129 PDAC tumors ≤ 2 cm (13.0%) and 867 PDAC tumors > 2 cm (87.0%). Normal controls had a mean age of 63.5 ± 14.8 years, with 46.2% female and 42.5% male subjects. Most normal scans were acquired in the portal-venous phase (90.2%), with a median slice thickness of 1.25 mm and a median in-plane spacing of 0.74 mm. The Southern California (North America) cohort included 791 patients, consisting of 521 diagnostic PDAC cases and 526 normal controls. Diagnostic cases included 110 PDAC tumors ≤ 2 cm (21.1%) and 411 PDAC tumors > 2 cm (78.9%), with a mean age of 66.9 ± 10.6 years. Normal controls had a mean age of 59.4 ± 18.1 years, with 48.3% female and 51.7% male subjects. CT scans exhibited increased heterogeneity in acquisition, with a median slice thickness of 2.55 mm and mixed contrast phases, including portal-venous (62.2%) and arterial (24.9%). The Central Europe cohort comprised 2,994 patients, including 367 diagnostic PDAC cases and 2,627 normal controls. The normal cohort comprises

1,227 females (46.7%), and 1,400 males (53.3%), with a mean age of 59.2 ± 15.6 years. All diagnostic PDAC tumors were pathology-confirmed, including 30 PDAC tumors ≤ 2 cm (8.2%) and 337 PDAC tumors > 2 cm (91.8%). The PDAC cohort comprises 177 females (48.2%), and 190 males (51.8%), with a mean age of 58.9 ± 13.9 years. For normal controls, scanner vendors included Toshiba (4.1%), Siemens (18.9%), Philips (18.9%), GE (52.3%), and Canon (5.8%), while for PDAC cases Toshiba (2.8%), Siemens (33.2%), Philips (16.5%), GE (46.0%), and Canon (1.5%). Both normal controls and diagnostic PDAC cases were exclusively of European ancestry. CT scans of normal control cohort were predominantly acquired in the portal-venous phase, with a median slice thickness of 1.25 mm and a median in-plane spacing of 0.76 mm, while diagnostic PDAC cohort were predominantly acquired in both arterial (48.5%) and portal-venous (51.5%) phases, with a median slice thickness of 1.25 mm and a median in-plane spacing of 0.77 mm. The Northern Europe cohort consisted of 560 diagnostic PDAC patients only and did not include true normal controls. PDAC tumor size distribution included 204 PDAC tumors ≤ 2 cm (36.4%) and 356 PDAC tumors > 2 cm (63.6%). All cases were histopathology-confirmed. CT scans were acquired exclusively in the portal-venous phase, with a median slice thickness of 2.0 mm and a median in-plane spacing of 0.73 mm. Scanner vendors included Philips (41.4%), Siemens (29.4%), Toshiba (23.5%), and GE (4.3%). The Eastern Asia cohort included 217 patients, comprising 112 diagnostic PDAC cases and 105 normal controls. Diagnostic cases had a mean age of 60.9 ± 9.4 years and included 91 PDAC tumors ≤ 2 cm (27.2%) and 243 PDAC tumors > 2 cm (72.8%). Normal controls had a mean age of 60.6 ± 11.1 years. Diagnostic scans included arterial (33.5%) and portal-venous (33.2%) phases, whereas normal scans were predominantly portal-venous (60.1%). The median slice thickness for diagnostic scans was 1.0 mm.

Prediagnostic and reader study cohort (Cohorts IV and V). Using electronic medical records (EHR) together with LLMs, we identified patients with biopsy-confirmed PDAC diagnosed between January 2006 and December 2020 in Northern California, United States ($n = 522$). We then retrieved abdominal CT examinations acquired for non-pancreatic indications 3–36 months before the index PDAC diagnosis, yielding 48 prediagnostic patients. We applied the same pipeline at two external hospitals in Eastern Asia, identifying an additional 111 prediagnostic patients. Prediagnostic examinations were required to have been interpreted as negative for PDAC in routine care, that is, no reported suspicion of pancreatic tumor. For patients with multiple eligible examinations, we included all scans acquired within 36 months before diagnosis that met the prediagnostic criteria. Each CT was re-reviewed by one of two radiologists (2–4 years post-residency experience) to confirm optimal image quality (e.g., minimal motion artifacts), contrast enhancement, and no evidence of pancreatitis, focal lesions, or common bile duct stents.

4.2 AI model: ePAI

ePAI is an automated system for detecting and localizing PDAC from contrast-enhanced abdominal CT scans, including prediagnostic scans acquired 3–36 months

before the first clinical diagnosis by radiologists. To improve interpretability and support lesion-level localization, ePAI is designed as a three-stage cascade that outputs spatial predictions rather than only patient-level scores.

Three-stage cascade. Stage 1 performs anatomical segmentation to localize the pancreas (head, body, tail), surrounding vessels (arteries and veins), and visible dilated ducts. Stage 2 detects and localizes all potential pancreatic lesions. Stage 3 classifies each detected lesion as PDAC, non-PDAC, or normal. This separation of segmentation, localization, and classification improves transparency and enables direct inspection of the predicted lesion location.

Training supervision and label confirmation. ePAI was trained on 1,598 contrast-enhanced abdominal CT scans from JHH. Ground-truth labels were confirmed by pathology for lesion cases and by two-year follow-up for normal controls. Radiologists provided pixel-wise annotations of the pancreas and lesion to supervise Stage 1 and Stage 2.

Synthetic lesions for small-tumor sensitivity. To increase sensitivity for small PDACs, ePAI was additionally trained on a large set of synthetic lesions with pixel-wise annotations automatically provided by generative AI. Synthetic lesions were used to enrich rare appearances and to expose the localization model to tumors near the lower limit of visibility.

Evaluation cohorts and clinical comparison. We evaluated ePAI on two clinically defined settings: (i) diagnostic scans, in which radiologists detected and reported PDAC, and (ii) prediagnostic scans, in which PDAC was initially overlooked and only detected in follow-up scans 3–36 months later. We assessed PDAC detection (PDAC versus normal) at the patient level and PDAC localization at the lesion level. Localization was considered correct when the predicted lesion location matched radiologists’ pixel-wise annotations or report-based localization. We further compared ePAI with radiologists, and measured the effect of assistance by ePAI, using a multi-reader study.

4.3 Evaluation metrics

PDAC detection. We evaluate PDAC detection as a binary classification task where ePAI determines whether each CT scan has a PDAC or not. For interpretability, we perform detection through semantic segmentation. By segmenting the tumor, ePAI provides localization, allowing radiologists to better understand and verify AI decisions. We consider that ePAI detected PDAC in a CT scan if the largest PDAC region segmented inside the pancreas has a maximum per-voxel PDAC probability greater than 50%. This definition of detection was used to compute the area under the receiver operating characteristic curve (AUC), sensitivity, specificity, accuracy, and balanced accuracy. We also stratified performance by T stage (T1–T4). Importantly, ePAI differentiates between PDAC and non-PDAC lesions, both present in our test sets.

PDAC localization. We considered a lesion correctly localized if the AI-generated tumor segmentation mask overlapped with the radiologist-drawn tumor segmentation mask. For test datasets without radiologist-drawn tumor masks, we considered a lesion correctly localized if the AI segmented it within the pancreatic sub-segment (head, body, or tail) that matched the lesion location described in the radiology report. We

then computed the accuracy as the number of correctly localized lesions divided by the total number of lesions in the test dataset.

Ablation studies. We performed two ablation studies to quantify the contribution of key design choices in ePAI. First, for lesion localization (Stage 2), we compared ePAI with a standalone nnU-Net trained directly for pancreatic lesion segmentation without Stage 1 initialization; lesion presence was defined by whether the model predicted any non-zero lesion voxels. Second, for lesion classification (Stage 3), we compared the full lesion-conditioned classifier with an image-level baseline that classifies the original CT directly (without using Stage 2 candidate lesions or lesion-level features).

Reader studies. We conducted a two-session reader study to assess radiologists' performance for pancreatic lesion detection and PDAC diagnosis on prediagnostic CT, and to test whether ePAI improves reader performance when used as an assistive tool. The two sessions were separated by a washout period of at least six month. A total of 30 readers from 5 institutions participated, including 3 pancreatic imaging specialists, 12 general radiologists and 15 radiology residents. Readers had a mean of 6.1 years of experience (range, 2–37 years) and reported reviewing a mean of 575 pancreatic CT examinations in the year before the study. Each reader interpreted 175 UCSF CT examinations, including 13 prediagnostic and 63 diagnostic CT scans with early PDAC, and 99 normal controls; readers were not informed of the class distribution. Readers were provided with the CT scan and patient age and sex. They answered three questions for each case: (1) whether a pancreatic lesion was present (yes/no); (2) if present, the lesion location within the pancreas; and (3) if present, whether the lesion was suspicious for PDAC, suspicious for a non-PDAC lesion or indeterminate.

In Session 1, readers reviewed cases using videos for visualization, without time constraints, and recorded their responses. In Session 2, readers interpreted the same cases with access to ePAI's outputs (e.g., PDAC segmentation masks). We quantified changes in reader performance between sessions. All PDAC and normal scans included in the reader study had optimal image quality and no signs of pancreatitis. Scans with biliary or pancreatic duct stents, particularly common bile duct stents, were excluded based on visual assessment by two radiologists.

Interpretability of the AI model. ePAI is interpretable at both the patient and lesion levels. For each examination, it outputs (i) a patient-level probability of abnormality, (ii) a lesion subtype prediction when abnormal, and (iii) voxel-wise segmentation masks of the detected lesion. In addition, Stage 1 provides multi-organ and vessel segmentations that localize the pancreas and surrounding anatomy, including visible ductal structures. These anatomical priors provide spatial context for ePAI's outputs and facilitate inspection of clinically relevant imaging cues. We quantified the spatial correspondence between predicted and reference segmentations using the localization sensitivity and the 95th percentile Hausdorff distance (HD95). To assess whether ePAI highlights clinically meaningful cues beyond the lesion itself, we also examined its predictions in the context of associated imaging findings and risk-related features, including pancreatic duct dilatation and related peripancreatic anatomical changes captured by the multi-organ and vessel segmentations.

Statistical analysis. For two group comparisons, we report the area under the receiver operating characteristic curve (AUC), sensitivity, specificity, positive predictive value (PPV), accuracy and F1 score. AUC was computed from model logits using `sklearn.metrics.roc_auc_score`. The remaining metrics were computed from thresholded predictions using `sklearn.metrics` (for example, `confusion_matrix` and `precision_recall_fscore_support`). We derived 95% confidence intervals (CIs) for sensitivity, specificity, accuracy and PPV using Wilson score intervals implemented with `statsmodels.stats.proportion.proportion_confint (method='wilson')`. We derived 95% CIs for AUC and F1 score using a nonparametric bootstrap with 1,000 resamples. All analyses were performed in Python using NumPy, SciPy, scikit-learn and statsmodels.

Acknowledgments. This work was supported by the National Institutes of Health (NIH) under Award Number R01EB037669, the Lustgarten Foundation for Pancreatic Cancer Research, and the Center for Biomolecular Nanotechnologies, Istituto Italiano di Tecnologia (73010, Arnesano, LE, Italy). We would like to thank the Johns Hopkins Research IT team in [IT@JH](#) for their support and infrastructure resources where some of these analyses were conducted, especially [DISCOVERY HPC](#); thank the HPC infrastructure and the Support Team at Fondazione Istituto Italiano di Tecnologia.

References

- [1] Siegel, R.L., Miller, K.D., Wagle, N.S., Jemal, A.: Cancer statistics, 2025. CA: A Cancer Journal for Clinicians **75**(1), 5–29 (2025) <https://doi.org/10.3322/caac.21900>
- [2] Mukherjee, S., Gevaert, O., Chari, S.T., *et al.*: Radiomics-based machine-learning models can detect pancreatic cancer on prediagnostic computed tomography scans at a substantial lead time before clinical diagnosis. Gastroenterology **163**(5), 1435–14467 (2022) <https://doi.org/10.1053/j.gastro.2022.07.009>
- [3] Hoogenboom, S.A., Voermans, R.P., Fölsch, U.R., Hooft, J.E., Besselink, M.G., Del Chiaro, M., Hackert, T., *et al.*: Pancreatic steatosis on computed tomography is an early imaging feature of pre-diagnostic pancreatic cancer: a preliminary study in overweight patients. Pancreatology **21**(3), 622–630 (2021) <https://doi.org/10.1016/j.pan.2021.01.009>
- [4] Konno, Y., Tsurusaki, M., Takahashi, T., Kubo, K., Sakamoto, N., Kitajima, K., Sugimura, K.: A retrospective preliminary study of intrapancreatic late enhancement as a noteworthy imaging finding in the early stages of pancreatic adenocarcinoma. European Radiology **33**(2), 1204–1214 (2023) <https://doi.org/10.1007/s00330-022-09003-2>
- [5] Chung, H.H., Lim, K.S., Park, J.K.: Clinical clues of pre-symptomatic pancreatic ductal adenocarcinoma prior to its diagnosis: a retrospective review of ct scans and laboratory tests. Clinical Practice **12**(6), 945–957 (2022) <https://doi.org/10.3390/clinpract12060098>

- [6] Toshima, F., Inoue, D., Yoshida, K., Yoneda, N., Minami, T., Hattori, E., Nakaura, T., Ueda, K., Kidoh, M., Tokunaga, K., *et al.*: Ct abnormalities of the pancreas associated with the subsequent diagnosis of clinical stage i pancreatic ductal adenocarcinoma more than 1 year later: a case-control study. *American Journal of Roentgenology* **217**(3), 579–589 (2021) <https://doi.org/10.2214/AJR.20.24651>
- [7] Singh, D.P., Sharma, P., Bhalla, A., Bhasin, D.K., Rana, S.S., Gupta, R.: Computerized tomography scan in pre-diagnostic pancreatic ductal adenocarcinoma: stages of progression and potential benefits of early intervention: a retrospective study. *Pancreatology* **20**(7), 1484–1490 (2020) <https://doi.org/10.1016/j.pan.2020.09.001>
- [8] Esteva, A., Kuprel, B., Novoa, R.A., Ko, J., Swetter, S.M., Blau, H.M., Thrun, S.: Dermatologist-level classification of skin cancer with deep neural networks. *Nature* **542**(7639), 115 (2017)
- [9] Li, W., Yuille, A., Zhou, Z.: How well do supervised models transfer to 3d image segmentation? In: International Conference on Learning Representations (2024). <https://github.com/MrGiovanni/SuPreM>
- [10] Bassi, P.R., Li, W., Chen, J., Zhu, Z., Lin, T., Decherchi, S., Cavalli, A., Wang, K., Yang, Y., Yuille, A.L., Zhou, Z.: Learning segmentation from radiology reports. In: International Conference on Medical Image Computing and Computer-Assisted Intervention, pp. 305–315 (2025). Springer. <https://github.com/MrGiovanni/R-Super>
- [11] Bassi, P.R., Zhou, X., Li, W., Płotka, S., Chen, J., Chen, Q., Zhu, Z., Przado, J., Hamamci, I.E., Er, S., Chen, X., Yavuz, M.C., Chou, Y.-C., Lin, T., Wang, K., Tang, Y., Cwikla, J.B., Decherchi, S., Cavalli, A., Yang, Y., Yuille, A.L., Zhou, Z.: Scaling artificial intelligence for multi-tumor early detection with more reports, fewer masks. *arXiv preprint arXiv:2510.14803* (2025)
- [12] Cao, K., Xia, Y., Yao, J., Han, X., Lambert, L., Zhang, T., Tang, W., Jin, G., Jiang, H., Fang, X., *et al.*: Large-scale pancreatic cancer detection via non-contrast ct and deep learning. *Nature medicine* **29**(12), 3033–3043 (2023)
- [13] Korfiatis, P., Suman, G., Patnam, N.G., Trivedi, K.H., Karbhari, A., Mukherjee, S., Cook, C., Klug, J.R., Patra, A., Khasawneh, H., *et al.*: Automated artificial intelligence model trained on a large data set can detect pancreas cancer on diagnostic computed tomography scans as well as visually occult preinvasive cancer on prediagnostic computed tomography scans. *Gastroenterology* **165**(6), 1533–1546 (2023)
- [14] Chen, P.-T., Chang, W.-Y., Chen, Y.-C., Hung, M.-C., Tsai, M.-H., Cheng, Y.-T., Kao, H.-L., Hsu, W.-H., Huang, C.-L., *et al.*: Pancreatic cancer detection on ct scans with deep learning: a nationwide population-based study. *Radiology*

- [15] Degand, L., Abi-Nader, C., Bône, A., Vétil, R., Placido, D., Chmura, P., Rohé, M.-M., De Masi, F., Brunak, S.: Validation of a pretrained artificial intelligence model for pancreatic cancer detection on diagnosis and prediagnosis computed tomography scans. *Investigative Radiology*, 10–1097 (2024)
- [16] Alves, N., Schuurmans, M., Rutkowski, D., Saha, A., Vendittelli, P., Obuchowski, N., Liedenbaum, M.H., Haldorsen, I.S., Molven, A., Yakar, D., et al.: Artificial intelligence and radiologists in pancreatic cancer detection using standard of care ct scans (panorama): an international, paired, non-inferiority, confirmatory, observational study. *The Lancet Oncology* (2025)
- [17] Chen, P.-T., Chang, D., Yen, H., Liu, K.-L., Huang, S.-Y., Roth, H., Wu, M.-S., Liao, W.-C., Wang, W.: Radiomic features at ct can distinguish pancreatic cancer from noncancerous pancreas. *Radiology: Imaging Cancer* **3**(4), 210010 (2021)
- [18] Qureshi, T.A., D’Souza, M.M., Sharma, R., Ranjan, P., Kakkar, A., Kumar, R.: Predicting pancreatic ductal adenocarcinoma using artificial intelligence analysis of pre-diagnostic computed tomography images. *Cancer Biomarkers* **33**(4), 487–496 (2022)
- [19] Xia, Y., Yu, Q., Chu, L., Kawamoto, S., Park, S., Liu, F., Chen, J., Zhu, Z., Li, B., Zhou, Z., Yuille, A.L., Fishman, E.K., Hruban, R.H.: The felix project: Deep networks to detect pancreatic neoplasms. *medRxiv* (2022)
- [20] Park, S., Chu, L., Fishman, E., Yuille, A., Vogelstein, B., Kinzler, K., Horton, K., Hruban, R., Zinreich, E., Fouladi, D.F., et al.: Annotated normal ct data of the abdomen for deep learning: Challenges and strategies for implementation. *Diagnostic and interventional imaging* **101**(1), 35–44 (2020)
- [21] Li, B., Chou, Y.-C., Sun, S., Qiao, H., Yuille, A., Zhou, Z.: Early detection and localization of pancreatic cancer by label-free tumor synthesis. *MICCAI Workshop on Big Task Small Data*, 1001-AI (2023)
- [22] Chen, Q., Chen, X., Song, H., Xiong, Z., Yuille, A., Wei, C., Zhou, Z.: Towards generalizable tumor synthesis. In: *IEEE/CVF Conference on Computer Vision and Pattern Recognition (CVPR)*, pp. 11147–11158 (2024). <https://github.com/MrGiovanni/DiffTumor>
- [23] Lai, Y., Chen, X., Wang, A., Yuille, A., Zhou, Z.: From pixel to cancer: Cellular automata in computed tomography. In: *International Conference on Medical Image Computing and Computer-Assisted Intervention (MICCAI)*, pp. 36–46 (2024). Springer
- [24] Li, X., Shuai, Y., Liu, C., Chen, Q., Wu, Q., Guo, P., Yang, D., Zhao, C., Bassi, P.R., Xu, D., Zhou, Z.: Text-driven tumor synthesis. *arXiv preprint*

- [25] Isensee, F., Jaeger, P.F., Kohl, S.A., Petersen, J., Maier-Hein, K.H.: nnu-net: a self-configuring method for deep learning-based biomedical image segmentation. *Nature Methods* **18**(2), 203–211 (2021)
- [26] Sharma, A., Kandlakunta, H., Nagpal, S.J.S., Feng, Z., Hoos, W., Petersen, G.M., Chari, S.T.: Model to determine risk of pancreatic cancer in patients with new-onset diabetes. *Gastroenterology* **155**(3), 730–739 (2018)
- [27] Dbouk, M., Katona, B.W., Brand, R.E., Chak, A., Syngal, S., Farrell, J.J., Kastrinos, F., Stoffel, E.M., Blackford, A.L., Rustgi, A.K., *et al.*: The multicenter cancer of pancreas screening study: impact on stage and survival. *Journal of clinical oncology* **40**(28), 3257–3266 (2022)
- [28] Blackford, A.L., Canto, M.I., Dbouk, M., Hruban, R.H., Katona, B.W., Chak, A., Brand, R.E., Syngal, S., Farrell, J., Kastrinos, F., *et al.*: Pancreatic cancer surveillance and survival of high-risk individuals. *JAMA oncology* **10**(8), 1087–1096 (2024)
- [29] Bray, F., Laversanne, M., Sung, H., Ferlay, J., Siegel, R.L., Soerjomataram, I., Jemal, A.: Global cancer statistics 2022: Globocan estimates of incidence and mortality worldwide for 36 cancers in 185 countries. *CA: a cancer journal for clinicians* **74**(3), 229–263 (2024)
- [30] Sung, H., Ferlay, J., Siegel, R.L., Laversanne, M., Soerjomataram, I., Jemal, A., Bray, F.: Global cancer statistics 2020: Globocan estimates of incidence and mortality worldwide for 36 cancers in 185 countries. *CA: a cancer journal for clinicians* **71**(3), 209–249 (2021)
- [31] Siegel, R.L., Kratzer, T.B., Giaquinto, A.N., Sung, H., Jemal, A.: Cancer statistics, 2025. *Ca* **75**(1), 10 (2025)
- [32] Nagtegaal, I.D., Odze, R.D., Klimstra, D., Paradis, V., Rugge, M., Schirmacher, P., Washington, K.M., Carneiro, F., Cree, I.A., *et al.*: The 2019 who classification of tumours of the digestive system. *Histopathology* **76**(2), 182 (2019)

Appendix A Supplementary Tables

Table A1: Characteristics of external *diagnostic* CT datasets across centers.

Variable	E.Coast	N.California	S.California	C.Europe	N.Europe	E.Asia
CT scan	363	996	521	712	560	334
Patient	363	996	521	367	560	112
Age, mean (SD)	—	65.4 (10.7)	66.9 (10.6)	58.9 (13.9)	68.0 (10.0)	60.9 (9.4)
Unknown (no.)	—	762	—	—	—	—
Sex						
Female, no. (%)	—	486 (48.8)	260 (49.3)	177 (48.2)	270 (48.2)	35 (31.3)
Male, no. (%)	—	509 (51.1)	267 (50.7)	190 (51.8)	290 (51.8)	77 (68.8)
Unknown (no.)	—	1 (0.1)	—	—	—	—
In-plane spacing, mm (IQR)	0.79 (0.70, 0.92)	0.74 (0.70, 0.81)	0.99 (0.74, 1.25)	0.77 (0.71, 0.83)	0.73 (0.68, 0.78)	0.74 (0.70, 0.79)
Slice thickness, mm (IQR)	2.50 (1.00, 5.00)	1.25 (1.25, 1.25)	1.32 (0.51, 2.00)	1.25 (0.80, 1.50)	2.00 (1.00, 3.00)	1.00 (1.00, 1.25)
Scanner, no. (%)						
TOSHIBA	—	—	—	20 (2.8)	131 (23.5)	—
SIEMENS	—	—	—	236 (33.2)	165 (29.4)	—
Philips	—	—	—	117 (16.5)	232 (41.4)	—
GE	—	—	—	328 (46.0)	24 (4.3)	—
Canon	—	—	—	11 (1.5)	6 (1.1)	—
Unknown	—	—	—	—	2 (0.4)	—
Confirmation, no. (%)						
Radiology	—	—	447 (84.8)	—	49 (8.8)	—
Pathology	—	—	80 (15.2)	—	118 (21.1)	—
Cytology	—	—	—	—	138 (24.6)	—
Histopathology	363 (100.0)	—	—	712 (100.0)	255 (45.5)	112 (100.0)
Race, no. (%)						
White	—	—	—	367 (100.0)	—	—
Black	—	—	—	—	—	—
Asian	—	—	—	—	—	112 (100.0)
Hispanic	—	—	—	—	—	—
Other	—	—	—	—	—	—
Unknown	—	—	—	—	—	—
Contrast phase, no. (%)						
Portal venous	21 (5.8)	—	331 (63.5)	367 (51.5)	560 (100.0)	111 (33.2)
Arterial	29 (8.0)	—	190 (36.5)	345 (48.5)	—	112 (33.5)
Unknown	313 (86.2)	—	—	—	—	111 (33.2)
T stage, no. (%)						
I	—	61 (6.1)	—	—	—	7 (6.3)
II	—	195 (19.6)	—	—	—	71 (63.4)
III	—	68 (6.8)	—	—	—	20 (17.9)
IV	—	438 (44.0)	—	—	—	14 (12.5)
Unknown	—	—	—	712 (100.0)	—	—
Diagnosis, no. (%)						
PDAC	363 (100.0)	996 (100.0)	521 (100.0)	367 (100.0)	560 (100.0)	112 (100.0)
≤ 2 cm	48 (13.2)	129 (13.0)	110 (21.1)	30 (8.2)	204 (36.4)	91 (27.2)
> 2 cm	315 (86.8)	867 (87.0)	411 (78.9)	337 (91.8)	356 (63.6)	243 (72.8)
Non-PDAC	—	—	—	—	—	—
≤ 2 cm	—	—	—	—	—	—
> 2 cm	—	—	—	—	—	—

Table A2: Characteristics of the internal (JHH) dataset used to develop and internally validate the ePAI system with a fixed train/test split.

Variable	Diagnostic CT scans (n = 3,440)		Normal CT scans (n = 1,645)	
	Training set	Test set	Training set	Test set
CT scan	2,098	1,342	1,046	599
Patient	1,058	695	533	303
Age, mean (SD)	62.3 (12.7)	66.2 (10.6)	46.2 (12.9)	47.7 (12.0)
Sex				
Female, no. (%)	455 (43.0)	111 (16.0)	193 (36.2)	109 (36.0)
Male, no. (%)	505 (47.7)	98 (14.1)	294 (55.2)	192 (63.4)
Unknown, no. (%)	98 (9.3)	486 (69.9)	46 (8.6)	2 (0.7)
In-plane spacing, mm (IQR)	0.73 (0.68, 0.79)	0.74 (0.68, 0.80)	0.68 (0.62, 0.73)	0.71 (0.67, 0.77)
Slice thickness, mm	0.5	0.5	0.5	0.5
Race				
White, no. (%)	63 (6.0)	1 (0.1)	381 (71.5)	227 (74.9)
Black, no. (%)	10 (0.9)	0 (0.0)	43 (8.1)	51 (16.8)
Asian, no. (%)	3 (0.3)	0 (0.0)	13 (2.4)	13 (4.3)
Other, no. (%)	3 (0.3)	0 (0.0)	16 (3.0)	10 (3.3)
Unknown, no. (%)	979 (92.5)	694 (99.9)	80 (15.0)	2 (0.7)
Contrast phase				
Portal venous, no. (%)	1,046 (49.9)	670 (49.9)	523 (50.0)	299 (49.9)
Arterial, no. (%)	1,052 (50.1)	672 (50.1)	523 (50.0)	300 (50.1)
T stage				
I, no. (%)	144 (13.6)	26 (3.7)	—	—
II, no. (%)	198 (18.7)	56 (8.1)	—	—
III, no. (%)	186 (17.6)	33 (4.7)	—	—
IV, no. (%)	23 (2.2)	7 (1.0)	—	—
Unknown, no. (%)	507 (47.9)	573 (82.4)	—	—
T grade				
I, no. (%)	191 (18.1)	7 (1.0)	—	—
II, no. (%)	288 (27.2)	90 (12.9)	—	—
III, no. (%)	165 (15.6)	76 (10.9)	—	—
IV, no. (%)	1 (0.1)	3 (0.4)	—	—
Unknown, no. (%)	413 (39.0)	519 (74.7)	—	—
Diagnosis				
PDAC, no. (%)	576 (54.4)	288 (41.4)	—	—
≤ 2 cm, no. (%)	91 (15.8)	50 (17.4)	—	—
> 2 cm, no. (%)	485 (84.2)	238 (82.6)	—	—
Non-PDAC, no. (%)	482 (45.6)	407 (58.6)	—	—
≤ 2 cm, no. (%)	194 (40.2)	214 (52.6)	—	—
> 2 cm, no. (%)	288 (59.8)	193 (47.4)	—	—
Dilated duct				
Yes, no. (%)	211 (19.9)	263 (37.8)	0 (0.0)	0 (0.0)
No, no. (%)	847 (80.1)	432 (62.2)	533 (100.0)	303 (100.0)
Death as of Aug. 2022				
Yes, no. (%)	240 (22.7)	94 (13.5)	1 (0.2)	0 (0.0)
No, no. (%)	720 (68.1)	115 (16.5)	484 (90.8)	301 (99.3)
Unknown, no. (%)	98 (9.3)	486 (69.9)	48 (9.0)	2 (0.7)
Smoking history				
Yes, no. (%)	34 (3.2)	1 (0.1)	1 (0.2)	0 (0.0)
No, no. (%)	45 (4.3)	0 (0.0)	32 (6.0)	0 (0.0)
Unknown, no. (%)	979 (92.5)	694 (99.9)	500 (93.8)	303 (100.0)

Table A3: Characteristics of external *normal* CT datasets across centers.

Variable	E.Coast	N.California	S.California	C.Europe	N.Europe	E.Asia
CT scan	80	952	526	2,818	1,386	163
Patient	80	952	526	2,627	1,386	105
Age, mean (SD)	46.8 (16.7)	63.5 (14.8)	59.4 (18.1)	59.2 (15.6)	58.7 (16.5)	60.6 (11.1)
Unknown (no.)	—	—	—	—	—	—
Sex						
Female, no. (%)	27 (33.8)	440 (46.2)	243 (48.3)	1,227 (46.7)	621 (44.8)	44 (41.9)
Male, no. (%)	53 (66.2)	405 (42.5)	260 (51.7)	1,400 (53.3)	765 (55.2)	61 (58.1)
Unknown (no.)	—	107 (11.2)	—	—	—	0 (0.0)
In-plane spacing, mm	0.86 (0.78, 0.94)	0.74 (0.70, 0.82)	0.92 (0.74, 0.91)	0.76 (0.70, 0.84)	0.74 (0.69, 0.78)	0.78 (0.72, 0.85)
Slice thickness, mm	1.00 (1.00, 1.00)	1.25 (1.25, 1.25)	2.55 (2.00, 5.00)	1.25 (1.00, 1.25)	1.50 (1.50, 2.40)	5.00 (5.00, 5.00)
Scanner, no. (%)						
TOSHIBA	—	—	—	116 (4.1)	517 (37.3)	—
SIEMENS	—	—	—	533 (18.9)	768 (55.4)	—
Philips	—	—	—	534 (18.9)	78 (5.6)	—
GE	—	—	—	1,473 (52.3)	21 (1.5)	—
Canon	—	—	—	162 (5.8)	1 (0.1)	—
Unknown	—	—	—	—	1 (0.1)	—
Confirmation, no. (%)						
Radiology	80 (100.0)	952 (100.0)	526 (100.0)	2,170 (82.6)	1,169 (84.3)	105 (100.0)
Pathology	—	—	—	—	86 (6.2)	—
Cytology	—	—	—	—	40 (2.9)	—
Histopathology	—	—	—	457 (17.4)	91 (6.6)	—
Race, no. (%)						
White	—	—	—	2,627 (100.0)	—	—
Black	—	—	—	—	—	—
Asian	—	—	—	—	—	105 (100.0)
Hispanic	—	—	—	—	—	—
Other	—	—	—	—	—	—
Unknown	—	—	—	—	—	—
Contrast phase, no. (%)						
Portal venous	80 (100.0)	859 (90.2)	327 (62.2)	2,627 (93.2)	1,386 (100.0)	98 (60.1)
Arterial	—	93 (9.8)	131 (24.9)	191 (6.8)	—	65 (39.9)
Unknown	—	—	68 (12.9)	—	—	—

Table A4: Reader experience in interpreting pancreatic and general abdominal CT scans for the reader study.

No.	Reader ID	Experience (years)	CTs read per year	Pancreatic CTs read per year	Training / Expertise
1	Specialist 1 (S1)	37	600	200	Pancreatic radiology
2	Specialist 2 (S2)	13	800	300	Pancreatic radiology
3	Specialist 3 (S3)	9	700	300	Pancreatic radiology
4	General 1 (G1)	12	12,000	1,000	General radiology
5	General 2 (G2)	24	14,000	2,000	General radiology
6	General 3 (G3)	7	8,000	1,000	General radiology
7	General 4 (G4)	6	9,000	1,000	General radiology
8	General 5 (G5)	4	13,000	1,000	General radiology
9	General 6 (G6)	5	18,000	2,400	General radiology
10	General 7 (G7)	5	10,000	1,200	General radiology
11	General 8 (G8)	8	12,000	1,000	General radiology
12	General 9 (G9)	6	9,000	1,000	General radiology
13	General 10 (G10)	5	7,000	800	General radiology
14	General 11 (G11)	5	7,000	600	General radiology
15	General 12 (G12)	4	3,000	300	General radiology
16	Resident 1 (R1)	2	900	100	General radiology
17	Resident 2 (R2)	4	4,000	600	General radiology
18	Resident 3 (R3)	3	6,000	800	General radiology
19	Resident 4 (R4)	2	4,500	400	General radiology
20	Resident 5 (R5)	2	2,000	150	General radiology
21	Resident 6 (R6)	2	1,500	100	General radiology
22	Resident 7 (R7)	2	1,600	100	General radiology
23	Resident 8 (R8)	2	800	100	General radiology
24	Resident 9 (R9)	2	1,000	100	General radiology
25	Resident 10 (R10)	2	1,100	100	General radiology
26	Resident 11 (R11)	2	700	100	General radiology
27	Resident 12 (R12)	2	500	100	General radiology
28	Resident 13 (R13)	2	600	100	General radiology
29	Resident 14 (R14)	2	800	100	General radiology
30	Resident 15 (R15)	2	1,100	200	General radiology

Table A5: Overall PDAC detection performance across institutions. Sensitivity, specificity, and AUC are reported in percentage (%). The number of evaluated patients is reported per site.

cohort	site	# of patients	Sensitivity	Specificity	AUC
Internal	JHH	581	97.1	98.7	98.5
External	East Coast	446	98.9	96.2	99.4
	Northern California	1,921	97.4	88.6	97.9
	Southern California	791	97.7	89.8	—
	Central Europe	2,994	94.3	87.1	95.5
	Northern Europe	560	98.9	—	—
	Eastern Asia	497	98.8	92.0	99.4

Table A6: PDAC detection performance across institutions. Results are reported separately for small (diameter ≤ 2 cm) and large (diameter > 2 cm) tumors. Sensitivity and specificity are reported in percentage (%). The number of evaluated PDAC patients is reported per site.

size	site	# of patients	Sensitivity	Specificity
<i>Small PDAC (diameter ≤ 2 cm)</i>				
	Internal (JHH)	43	95.3	98.7
	East Coast	48	97.9	96.2
	Northern California	129	89.9	88.6
	Southern California	108	94.4	89.8
	Central Europe	30	86.7	87.1
	Northern Europe	204	98.9	—
	Eastern Asia	91	100.0	92.0
<i>Large PDAC (diameter > 2 cm)</i>				
	Internal (JHH)	236	97.5	98.7
	East Coast	315	99.0	96.2
	Northern California	867	98.5	88.6
	Southern California	408	98.5	89.8
	Central Europe	337	95.0	87.1
	Northern Europe	356	98.9	—
	Eastern Asia	243	100.0	92.0